INTERPRETATION OF SCANING TUNNELING MICROSCOPY IMAGES VIA DENSITY FUNCTIONAL CALCULATIONS

Yves Ferro and Alain Allouche, Université de Provence, Centre de Saint Jérôme, 13397 Marseille Cedex 20, France

This paper is devoted to the study of the electronic structure of a single atomic vacancy on graphite. Interpretation of STM images on graphite surfaces is subsequently investigated. The (0001) surface of graphite is model by a single, then a double a graphene sheets. Tersoff and Hamann [Tersoff] have showed that under reasonable approximation, the STM topography is a map of constant charge density at E_F (ρ_{STM}). Therefore, the interpretation of STM images is related to the knowledge of the electronic structure of the graphite surface. Thus, the electronic band structure, density of states and constant charge density near E_F have been calculated in order to better assign and interpret the main features of STM images of an atomic vacancy on graphite. The interlayer interaction plays a crucial role in the interpretation of STM images. A double layer model was subsequently considered and the impact of the interlayer interaction analyzed [Ferro].

From an experimental point of view, atomic vacancies on graphite are characterized by bright spots in the vicinity of the defect, ($\sqrt{3}\times\sqrt{3}$) *R*30° modulation of the local electronic density near the Fermi level, and a third-order symmetry structure) to the electronic band structure of the defective graphite surface [Ruffieux05, Ruffieux00, Kelly, Mizes, Lee, El-Barbary].

Methods

Calculations were performed in a periodic approach using the Perdew, Burke and Ernzerhof GGA functional for exchange and correlation [Perdew] as implemented in the ABINIT package [Abinit]. Trouiller - Martins pseudopotentials [Trouillet] were used with a plane-waves basis set expansion cutoff of 25 Hartrees (680 eV).
Applying a small bias voltage V_{bias} between the tip and the sample yields a tunneling current whose density is proportional to ρ_{STM} given by :

$$\rho_{STM}(r,V_{bias}) = \int_{E_F - eV_{bias}}^{E_F} \sum_{i}^{levels} \sum_{\vec{k}\in BZ} \left|\varphi_{i,\vec{k}}(\vec{r})\right|^2 \delta(E_{i,\vec{k}} - E)\, dE \qquad (1)$$

We have calculated ρ_{STM} within $\Delta E_{STM} = E_F \pm E$ with $E \approx 1$ eV.
We choose *3n*×*3n* unit cells in order the charge density waves (CDW) that formed on the vicinity of the vacancy do not destroy. Indeed, the wavelength of a $\varphi_{i,\vec{k}}(\vec{r})$ near E_F is $\lambda_F = 3/2\ a$. Thus, the CDWs in the vicinity of the defect are characterized by $\lambda = 3a$ wavelengths and form a ($\sqrt{3}\times\sqrt{3}$) R30° superstructure [Mizes].

The electronic structure of graphene with a vacancy

The perfect surface

STM scans the electronic density from wave functions associated to levels located at the $\overline{\mathrm{K}}$ corner of the surface BZ where the π and π^* bands connect. At this point, the two independent electronic one-electron wave functions, degenerated solutions of the Kohn Sham operator, may be written in the LCAO approximation as:

$$\varphi_{i,\vec{k}_f}(\vec{r}) = \frac{1}{\sqrt{N}} \sum_{\vec{R}} 2p_Z^{\alpha}(\vec{r}-\vec{R}) \exp(i\vec{k}_f.\vec{R}) \qquad \alpha = \mathrm{A, B} \qquad (2)$$

A and *B* refer to the two carbon atoms belonging to the surface unit cell. *A*-type atoms are located at (0, 0) on the corner of the unit cell and *B*-type are at $(\frac{1}{3},\frac{2}{3})$. Adding up all $\overline{\mathrm{K}}$ solutions of the BZ, we built four degenerated orthogonal electronic one-electron wave functions:

$$\varphi_{i,\vec{k}_f}(\vec{r}) = \frac{2}{\sqrt{N}} \sum_{\vec{R}} 2p_Z^{\alpha}(\vec{r}-\vec{R})\cos(\vec{k}_f.\vec{R})$$

$$\varphi_{i,\vec{k}_f}(\vec{r}) = \frac{2}{\sqrt{N}} \sum_{\vec{R}} 2p_Z^{\alpha}(\vec{r}-\vec{R})\sin(\vec{k}_f.\vec{R}) \qquad \alpha = \text{A, B} \qquad (3)$$

In Fig 1, we plotted the square modulus of those solutions for the *A*-atom in a 3×3 super-cell model. Each independent solution exhibits the (√3×√3) R30° superstructure while the summation of the *sine* and *cosine* square modulus solutions restores the original unit-cell. Thus, any perturbation destroying one of this contribution leads to the (√3×√3) R30° superstructure of the electronic density.

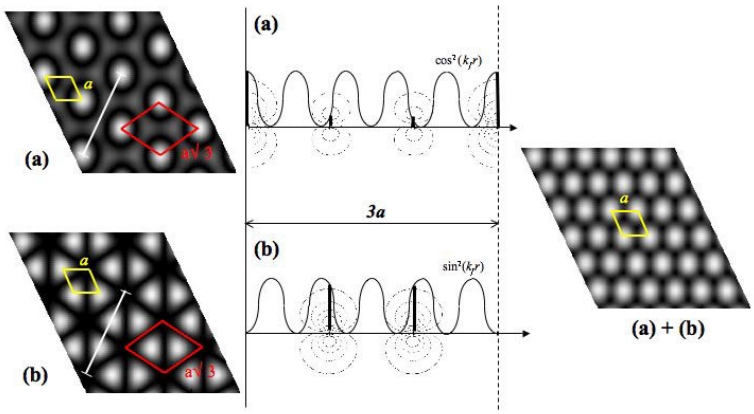

Figure 1. Square modulus of the (a) *cosine* and (b) *sine* wave function on *A*-type atoms, solutions of the Kohn Sham operator at the Fermi level ($\overline{\Gamma}$ point of the 2D BZ of a 3×3 supercell). (a) and (b) exhibit the (√3×√3) R30° modulation while their sum (a) + (b) have the unit-cell periodicity. $Sin^2(k_f r)$ and $cos^2(k_f r)$ are also shown and plotted along the white lines shown on the images.

The surface with a vacancy

In Fig. 2a, we plotted the band structure close to the Fermi level of a 6×6 model with an α vacancy. Fig 2b. shows an enlarged part of this band structure at the $\overline{\Gamma}$ point and near E_F:

(*m*) and (*n*) are the square modulus of the degenerated *sine* and *cosine* solutions of eq. 8.3 on *B*-type atoms at the Fermi level. As a consequence, the unit-cell still appears in the background of the STM image.

The *(l)* solution is 41 meV below E_F; It is the *sine* solution on *A*-type atoms with a node on the vacant site. It induces the (√3×√3) R30° modulation, which is superimposed on the image. The *cosine* solution leading to a maximal electronic density on the vacancy does not exist. This result is consistent with the proposals of Mize *et al.* [Mizes].

Two degenerate levels (*o*) and (*p*) are calculated 10 meV above E_F. As shown on the gray scale images these states are very localized on the vacant site. The dispersion of the electronic band to which they belong is weak: ΔE = 34 meV along $\overline{\Gamma} \rightarrow \overline{M} \rightarrow \overline{K}$. These are local states coming from the defect, and from which the peak at E_F arises in the DOSs of Fig. 8.1. These states are consistent with the presence of bright spots in the neighborhood of the vacancy.

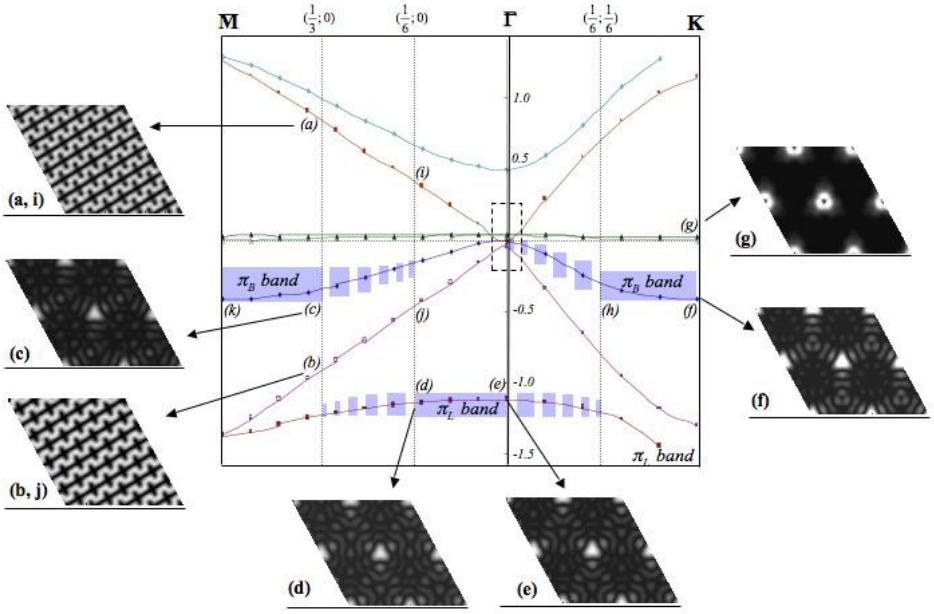

Figure 2a. The electronic band structure of the 6×6 model with an atomic vacancy on an *A*-type site in the center of the working cell. Cuts of the square modulus are shown as gray scale images are presented for some relevant point of the band structure from *(a)* to *(k)*. The three-branch star feature of the π_B and π_L bands are shown as shaded areas.

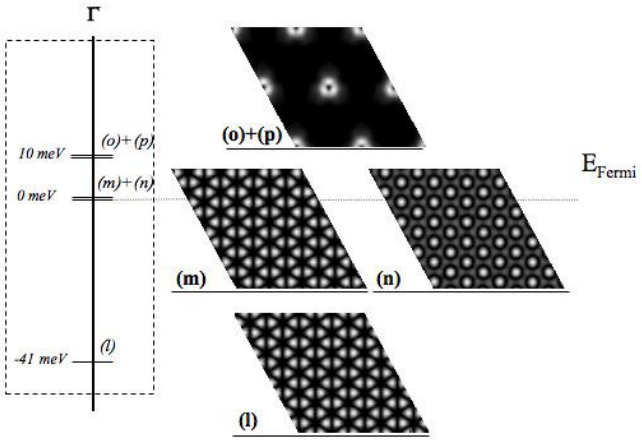

Figure 2b. Enlargement of the squared part in Fig. 3a at the $\overline{\Gamma}$ point.

At last, the three-branch star pattern is shown in shaded area in Fig. 2a. At the $\overline{\Gamma}$ point, the *(e)* level wave function get this pattern. However, this solution is very low in energy (1.14 eV below E_F) and does not belong to ρ_{STM}. Looking at the whole band structure, the three-branch star features jump from this low energy π_L band to the upper π_B band connecting the two degenerated *sine B (m)* and *cosine B (n)* solutions at $\overline{\Gamma}$. This third-order symmetry structure pattern will be observed or not, depending on the bias voltage imposes tothe tip.

Thus the local density of states ρ_{STM} was plotted at different ΔE_{STM} in Fig 3 for the 6×6 and 9×9 models. The features here presented are indeed observed in the image from Ruffieux *et al.* in Ref [Ruffieux00] and Ref [Ruffieux05].

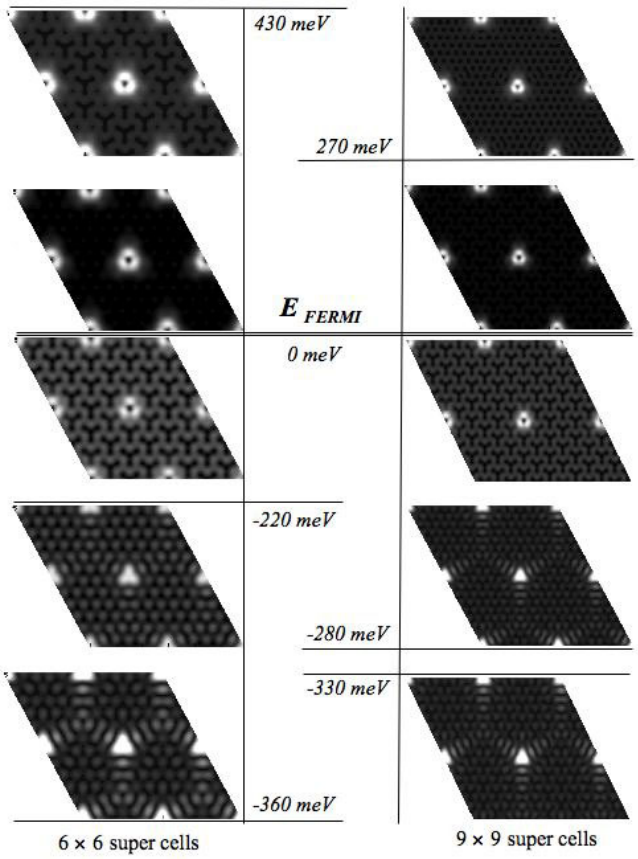

Figure 3. Calculated STM images for different domain in energy for the 6×6 and 9×9 models

The interlayer interaction.

The interlayer interaction was investigated on a two layer 6×6 model with graphite sheets separated by 3.35 Å and belonging to an AB stacking; the Brillouin zones were sampled in a 3×3×1 point mesh.

The main effect of the interlayer interaction is to produce a splitting of the solutions involving A-type atoms, while non-affecting those from B-type ones. All other properties from the graphene sheet remain roughly the same. The splitting induces bonding and anti-bonding interactions between the layers [Ferro].

The interlayer interaction induces the presence of the three-branch star feature everywhere in the BZ of the β vacancy, and particularly at the $\overline{\Gamma}$ point at an energy very close to E_F (-78.3 meV). In the case of α vacancy, the weaker dispersion of the π_B band making the three-branch star feature appears closer from E_F (above -218 eV) than on a graphite sheet.

We plotted ρ_{STM} in Fig 4 calculated at different energies for both α and β vacancies. They clearly exhibit different pattern and may be distinguish from each other.

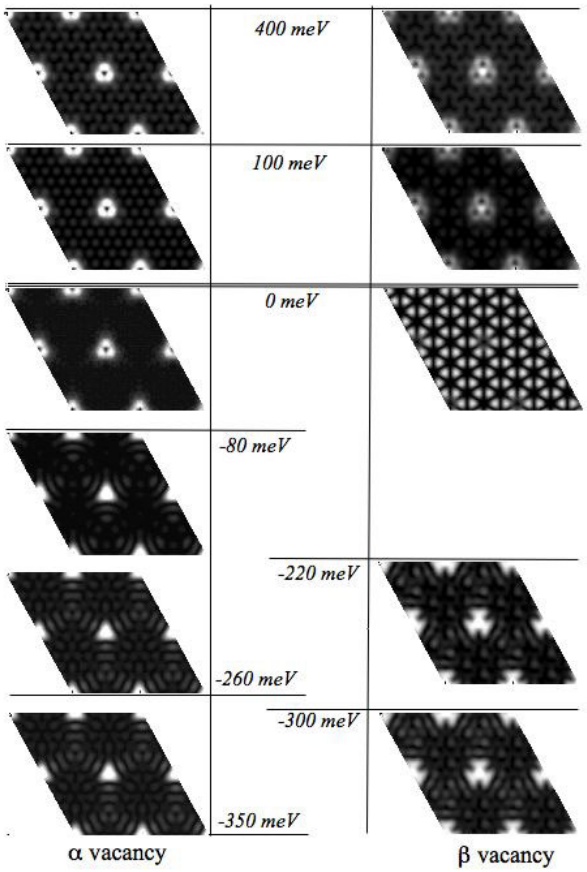

Figure 4. Calculated STM images for different domains in energy for the α and β vacancies.

The major difference is induced, on the β vacancy. At $\overline{\Gamma}$, the *Sin* B solution induces a (√3×√3) R30° modulation over the whole domain in energy we considered, on the contrary with the α vacancy. The three-branch star feature appears at low energy along the band connecting the *sin* B solution. In the α vacancies case, the three-branch star feature exists since 78.3 meV below E_F and is apparent along the whole band from $\overline{\Gamma}$ to $\overline{K}$ [Ferro]. Considering the broadening due to the tip electronic distribution, this feature may appear at low temperature starting from -55 meV. This result is in very good agreement with the findings of Ruffieux et al [Ruffieux00, Ruffieux05] who observed this pattern for bias voltage of 36 mV and 70 mV, respectively. They are alos consistent with the results from Hahn *et al.* [Hahn96, Hahn99] who observed similar images as those we found on an α vacancy at 100 meV with bias voltage of -36 and -60 mV (36 and 60 meV above E_F).

Kelly et al. [Kelly98] using a tight-binding model have calculated STM images for α and β vacancies. They found the three-branch star to be rotated by 60° from α to β vacancy. This result we reproduced (Fig 8.6) was indeed observed from an experimental point of view by Kushmerick et al. [Kushmerick99].

Conclusion

The models we built allowed us to calculate, within the DFT framework, the electronic structure of graphene and graphite bilayers with vacancies. We assign each main feature of STM images to some main features of the electronic structure of the surface near the Fermi level. The impact of the interlayer interaction was further investigated. It splits the solution above and below the Fermi level for the solutions involving the A-type atoms. On α vacancies, this causes the (√3×√3) R30° modulation based on A atoms to disappear while the three-branch star feature comes closer to the Fermi level. On the contrary, on a β vacancy, ρ_{STM} is dominated by the (√3×√3) R30° modulation based on B-type atoms while the unit-cell network based on A atoms is moved away from E_F.

In both cases, the local surface states with a high-density region centered on the defect are almost unaffected. Those results are in good agreement with experimental observation and allow differentiating α and β atomic vacancy on a graphite surface.

Bibliography

[Abinit] available from http://www.abinit.org
[Ferro] Y. Ferro and A. Allouche, Phys. Rev. B **75**, 155438 (2007).
[Hahn99] J.R. Hahn and H.Kang Phys. Rev. B **60**, 6007 (1999)
[Hahn96] J. R. Hahn, H.Kang, S. Song, and I. C. Jeon, Phys. Rev. B **53**, R1725 (1996).
[Kelly] K. F. Kelly, and N. J. Halas, Surf. Sci. **416** L1085 (1998).
[Kushmerick99] J. G. Kushmerick, K. F. Kelly, H. P. Rust, N. J. Halas, and P. S. Weiss, J. Phys. Chem. B **103**, 1619 (1999).
[Mizes] H. A. Mizes, and J. S. Foster, Science **244** 559 (1989).
[Perdew] J. P. Perdew, K. Burke and M. Ernzerhof, Phys. Rev. Lett. **77** (1996) 3865.
[Ruffieux00] P. Ruffieux, O. Gröning,, P. Scwaller, L. Schlapbach, and P. Gröning, Phys. Rev. Lett. **84** 4910 (2000)
[Ruffieux05] P. Ruffieux, M. Melle-Franco, O. Gröning, M. Bielmann, F. Zerbetto, and P. Gröning, Phys. Rev. B **71** 153403 (2005).
[Tersoff] J. Tersoff, and D. R. Haman, Phys. Rev. B **31,** 105 (1985).
[Trouillet] N. K. Trouiller, J. L. Martins, Phys. Rev. B **43** (1991) 1993.